$\alpha v \beta 3$ integrin spatially regulates VASP and RIAM to control adhesion dynamics and migration

Daniel C. Worth,¹ Kairbaan Hodivala-Dilke,² Stephen D. Robinson,² Samantha J. King,¹ Penny E. Morton,¹ Frank B. Gertler,³ Martin J. Humphries,⁴ and Maddy Parsons¹

Integrins are fundamental to the control of protrusion and motility in adherent cells. However, the mechanisms by which specific members of this receptor family cooperate in signaling to cytoskeletal and adhesion dynamics are poorly understood. Here, we show that the loss of $\beta 3$ integrin in fibroblasts results in enhanced focal adhesion turnover and migration speed but impaired directional motility on both 2D and 3D matrices. These motility defects are coupled with an increased rate of actin-based protrusion. Analysis of downstream signaling events reveals that loss of $\beta 3$ integrin results in a loss of

protein kinase A-dependent phosphorylation of the actin regulatory protein vasodilator-stimulated phosphoprotein (VASP). Dephosphorylated VASP in $\beta3$ -null cells is preferentially associated with Rap1-GTP-interacting adaptor molecule (RIAM) both in vitro and in vivo, which leads to enhanced formation of a VASP-RIAM complex at focal adhesions and subsequent increased binding of talin to $\beta1$ integrin. These data demonstrate a novel mechanism by which $\alpha\nu\beta3$ integrin acts to locally suppress $\beta1$ integrin activation and regulate protrusion, adhesion dynamics, and persistent migration.

Introduction

Cell migration is a tightly regulated process involving the spatial and temporal coordination of protrusion, adhesion, and contraction (Ridley et al., 2003). Integrins are a family of heterodimeric transmembrane receptors that form the main cell–ECM contact point in many cell types. As such, integrins are one of the primary components in the control of cell adhesion and protrusion both from the ligand-binding side and the formation of signaling platforms at the cytoplasmic face of the plasma membrane (Hynes, 2002). In adherent cells, it is widely known that both $\beta 1$ and $\beta 3$ integrins contribute to both normal cell migration and cancer cell invasion (Ramsay et al., 2007; Caswell and Norman, 2008). $\beta 1$ and $\beta 3$ integrins are also proposed to act upon one another through transdominant inhibition, resulting in suppression of signaling, possibly through competition for key integrin activation proteins such as talin

Correspondence to Maddy Parsons: maddy.parsons@kcl.ac.uk

Abbreviations used in this paper: CDM, cell-derived matrix; Ena/VASP, Enabled/protein vasodilator-stimulated phosphoprotein; FLIM, fluorescence lifetime imaging microscopy; FN, fibronectin; FRET, fluorescence resonance energy transfer; GAPDH, glyceraldehyde 3-phosphate dehydrogenase; RIAM, Rap1-GTP-interacting adaptor molecule; WT, wild type.

(Calderwood et al., 2004). As both receptors share extracellular ligands, as well as cytoplasmic binding partners such as the cytoskeletal proteins talin and filamin (Arnaout et al., 2007), the manner in which these subunits individually contribute to cell motility is unclear.

Previous studies have localized $\alpha v \beta 3$ integrin within small dynamic focal complexes at the leading edge of motile fibroblasts, whereas $\beta 1$ is found predominantly in larger focal adhesions that act to stabilize new actin-based membrane protrusions and the cell body (Zamir et al., 2000; Zaidel-Bar et al., 2003). Both adhesion types are required to disassemble in order to allow efficient cell migration to occur, with smaller focal complexes displaying more rapid turnover than focal adhesions (Broussard et al., 2008). In order for cells to undergo persistent motility, adhesion dynamics must also be coordinated with the assembly of new F-actin–containing protrusions, which are in

© 2010 Worth et al. This article is distributed under the terms of an Attribution–Noncommercial–Share Alike–No Mirror Sites license for the first six months after the publication date (see http://www.rupress.org/terms). After six months it is available under a Creative Commons License (Attribution–Noncommercial–Share Alike 3.0 Unported license, as described at http://creativecommons.org/licenses/by-nc-sa/3.0/).

Downloaded from http://rupress.org/jcb/article-pdf/189/2/369/1573586/jcb_200912014.pdf by guest on 02 December 2025

¹Randall Division of Cell and Molecular Biophysics, King's College London, London SE1 1UL, England, UK

²Centre for Tumour Biology, Cancer Research UK Clinical Centre, Institute of Cancer, Bart's and The London School of Medicine and Dentistry, London EC1M 6BQ, England, UK

³Koch Institute and Department of Biology, Massachusetts Institute of Technology, Cambridge, MA 02139

⁴Wellcome Trust Centre for Cell-Matrix Research, Faculty of Life Sciences, University of Manchester, Manchester M13 9PT, England, UK

turn under the control of several actin-nucleating and elongating molecules (Le Clainche and Carlier, 2008). One such family are the Enabled/protein vasodilator-stimulated phosphoprotein (Ena/VASP) proteins, which act to antagonize capping protein, induce actin filament elongation (Sechi and Wehland, 2004), and, additionally, localize to focal adhesions. Rap1-GTP-interacting adaptor molecule (RIAM) is a member of the Mig-10/RIAM/ Lamellipodin (MRL) family of adaptor proteins (Lafuente et al., 2004). RIAM overexpression induces β1 and β2 integrinmediated cell adhesion and cell spreading; RIAM knockdown reduces Rap1-dependent cell adhesion and integrin activation, and leads to a reduction in cellular F-actin content (Lafuente et al., 2004; Han et al., 2006). RIAM is a binding partner for both talin and VASP, and RIAM association with talin has recently been shown to modulate integrin activation (Lee et al., 2009). However, the role of the VASP-RIAM complex in regulating talin dynamics, integrin activation, and motility remains unknown.

Here, we provide evidence that $\alpha v \beta 3$ integrin promotes efficient cell motility through two mechanisms. Fibroblasts lacking \(\beta \) integrin show increased F-actin content and enhanced rates of membrane protrusion. This is coincident with the presence of constitutively dephosphorylated VASP that associates with RIAM at peripheral focal adhesions and promotes enhanced formation of a RIAM-talin complex. Moreover, \(\beta \)3 expression and localization to the leading edge suppresses local activation of β1 integrin. Loss of β3 results in an increase in VASP/RIAM-dependent peripheral active β1 integrincontaining adhesions that show increased rates of assembly and disassembly compared with those in wild-type (WT) cells. These findings suggest that $\alpha v\beta 3$ integrin contributes toward regulation of actin dynamics at the leading edge as well as negatively regulating β1 activation, adhesion dynamics, and stable protrusion.

Results

Fibroblasts lacking β 3 integrin have altered adhesion localization and dynamics

To determine whether β3 integrin is required for correct spatial adhesion organization, fibroblasts isolated from WT and β 3-deficient (β 3-/-) animals (Hodivala-Dilke et al., 1999) were plated on fibronectin (FN) and stained with antibodies to \$1 and β3 and the focal adhesion markers vinculin (Fig. 1 A), zyxin, paxillin, or talin (not depicted). Confocal images and quantitative analysis revealed that cells lacking \(\beta \) integrin formed small, more peripheral focal adhesions and fewer large adhesions beneath the cell body as compared with WT cells (Fig. 1, A and B), but did not show a difference in total spread area on FN (not depicted). WT phenotypes were restored in all cases in β 3-/- rescued with stable expression of a human β 3-GFP construct. Western blotting showed an increase in levels of talin in cells lacking \(\beta \), which were also restored to WT levels in β3-GFP cells (Fig. S1 B). No other changes in levels of other focal adhesion proteins or other integrin subunits were observed (Fig. S1 A).

Control of cell adhesion formation in vivo is regulated by the architecture of the surrounding ECM. To determine whether the differences in adhesion localization in the $\beta 3$ -/- cells were also evident in a more complex 3D environment, we plated both WT and $\beta 3-/-$ cells on cell-derived matrices (CDMs; Cukierman et al., 2001). Confocal images of fixed cells in CDM stained for active \(\beta 1 \) integrin, paxillin, and FN also showed increased numbers of peripheral matrix-associated adhesions in β3-/- (Fig. 1 C), which suggests that spatial control of adhesion formation is altered in these cells irrespective of matrix cues. To investigate whether the altered adhesion localization also translated to a functional change in adhesion turnover, WT and $\beta 3$ —/— cells expressing low levels of GFP-talin (Fig. 1 D) or GFP-vinculin (not depicted) were plated on 2D FN and imaged by time-lapse fluorescence microscopy to monitor adhesion dynamics. Analysis of adhesion intensity over time and calculation of rate constants revealed that loss of \(\beta \) resulted in a higher rate of adhesion assembly and disassembly compared with WT or β3-GFP rescued β3-null cells (Fig. 1 D). Additional quantification of the number of dynamic adhesions seen during the imaging period demonstrated that significantly more adhesions disassembled in β3-/- compared with WT cells (Fig. S2 A). To determine whether the ECM environment could alter this phenomenon, we also performed analysis of adhesion dynamics in cells in CDM. Interestingly, data revealed two populations of adhesions in both cell types in CDM (Fig. 1 E): one "slow" population showing rate constants of assembly and disassembly in the order of 0.1–0.3 min⁻¹, and a "fast" population of 0.4–0.9 min⁻¹. Of note, the fast population showed significantly faster adhesion dynamics than all adhesion in cells on 2D FN. Importantly, $\beta 3-/-$ cells showed higher rates of both assembly and disassembly in CDM, and this difference was more striking within the slow adhesion population. This data suggests that \(\beta \) can act to stabilize focal adhesions in fibroblasts.

Talin is known to bind directly to the cytoplasmic domain of $\beta 1$ integrin, leading to inside-out activation (Tadokoro et al., 2003), and changes in dynamic behavior of talin in the absence of $\beta 3$ may contribute toward the increased activation of $\beta 1$. To determine whether loss of $\beta 3$ led to changes $\beta 1$ activation in these cells, we performed cell surface FACS analysis using antibodies to detect either total or active (9EG7) $\beta 1$. Interestingly, despite similar levels of total protein and membrane levels of $\beta 1$, $\beta 3-/-$ cells showed significantly higher active $\beta 1$ at the cell surface compared with WT cells (Fig. 1 F). These data suggest that $\beta 3$ integrin may act to suppress the activation of $\beta 1$ in fibroblasts.

β3 integrin regulates fibroblast migration speed and persistence

Previous studies have shown that localization and recycling of $\beta 3$ integrin is important in dictating polarized cell movement (Ballestrem et al., 2001; Danen et al., 2005; White et al., 2007). To determine whether genetic loss of $\beta 3$ in fibroblasts affects migration, we imaged WT and $\beta 3-/-$ cells plated on 2D FN or in CDM by phase-contrast time-lapse microscopy, and quantified the speed and persistence of migration. Fig. 1 (G and H) and Fig. S2 B show quantification from videos of WT and $\beta 3-/-$ cells on FN (Videos 1 and 2), which

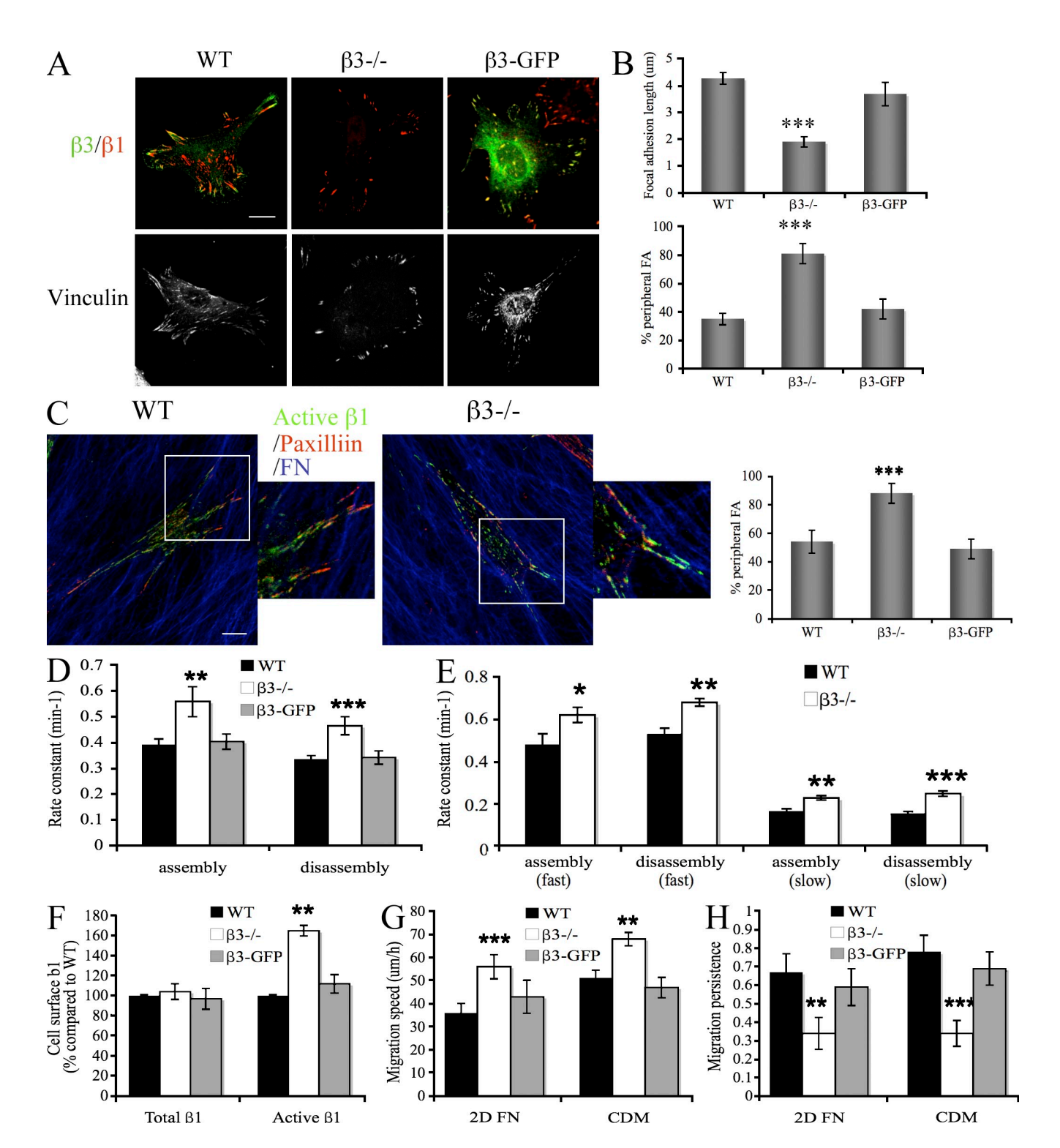


Figure 1. Loss of $\beta 3$ leads to formation of peripheral adhesions and enhanced migration. (A) Confocal images of WT, $\beta 3-/-$, or $\beta 3$ -GFP cells plated on FN and costained for (top panels) $\beta 3$ (FITC or GFP, green) and $\beta 1$ (Alexa Fluor 568, red) or vinculin (bottom; shown in black and white). Bar, 10 μ m. (B) Quantification of focal adhesion length, percentage of peripheral adhesions, and area/cell from confocal images. Adhesions were quantified from at least 100 cells over three independent experiments. Data are shown as mean \pm SEM. (C, left) Confocal images of WT and $\beta 3-/-$ plated on CDMs and costained for active $\beta 1$ (9EG7-FITC, green), paxillin (Alexa Fluor 568, red), and FN (Alexa Fluor 633, blue). Insets show enlarged views of the boxed regions. Bar, 10 μ m. (right) The bar graph shows quantification of the percentage of peripheral adhesions from confocal images. Adhesions were quantified from at least 30 cells over three independent experiments. Data are shown as mean \pm SEM. (D and E) Rate constants of focal adhesion dynamics in WT, $\beta 3-/-$, or $\beta 3$ -GFP cells plated on 2D FN (D) or CDM (E). Data were quantified from time-lapse videos of cells expressing GFP- or mCherry-talin. Data are expressed as min⁻¹ \pm SEM. Data were quantified from a minimum of 200 adhesions per cell type over four experiments. (F) WT, $\beta 3-/-$, and $\beta 3$ -GFP cells were fixed and stained for cell surface levels of total or active $\beta 1$ integrin (MB 1.2 or 9EG7, respectively) and analyzed by FACS. Data are presented as the mean percentage of active cell surface levels of total or active $\beta 1$ integrin (MB 1.2 or 9EG7, respectively) and analyzed by FACS. Data are presented as the mean percentage of active cell surface levels of total or active $\beta 1$ integrin (MB 1.2 or 9EG7, respectively) and analyzed by FACS. Data are presented as the mean percentage of active cell surface levels of total or active $\beta 1$ integrin (MB 1.2 or 9EG7, respectively) and analyzed by FACS. Data are presented independent experiments. Data

demonstrates that $\beta 3-/-$ cells display an increase in migration speed but a decreased persistence of movement. This phenotype was also evident in cells migrating within CDM, where β3-/- cells show multiple protrusions and WT cells display an elongated morphology and migrate persistently along matrix fibers (seen as black lines in the phase-contrast images; Videos 3 and 4). These data are in agreement with previous studies in proposing a role for β3 in negative regulation of migration speed (Danen et al., 2005; Reynolds et al., 2005; White et al., 2007) and suggest that β3 additionally functions to promote directional persistence of motility.

Loss of β 3 integrin results in increased cellular F-actin

Adhesion dynamics can contribute to the stability of the F-actin cytoskeleton and in turn regulate mechanical coupling of the cell to the ECM during cell motility (Vicente-Manzanares et al., 2009). To address whether the changes in motility in $\beta 3-/$ cells were coupled with altered actin assembly, we measured total F-actin levels in WT and $\beta 3$ -/- cells by both FACS and Western blotting. Surprisingly, both types of analyses revealed a significant increase in insoluble or F-actin in β3-/- cells compared with WT (Fig. 2, A and B), which suggests that loss of β3 leads to stabilization of actin filaments. To study membrane protrusion in more detail, WT, β 3-GFP, and β 3-/- cells were imaged by phase-contrast time-lapse microscopy over short time periods and subjected to kymograph analysis to quantify membrane protrusion rates. Live imaging revealed that $\beta 3-/-$ cells exhibit multiple unstable protrusions, and quantification demonstrated a significant increase in both the protrusion rate and the amount of protrusion per cell area in β3-/- cells compared with WT or β3-GFP rescue cells (Fig. 2 C). This altered protrusive behavior was also evident in $\beta 3-/-$ cells transfected with GFP-actin and monitored by fluorescence time-lapse microscopy (Fig. 2 D and Videos 5 and 6). Moreover, analysis of Alexa Fluor 568–labeled G-actin incorporation in live WT or $\beta 3-/$ cells also revealed an increase in free barbed end formation in cells lacking \(\beta \) integrin (Fig. 2 E). Together, these data suggest that the presence of \(\beta \) can act to suppress and stabilize the formation of F-actin protrusions. These data combined with the observed increases in \$1 integrin activation in the absence of \$3 provide one possible explanation for the enhanced migration speed and loss of persistent movement seen in these cells. Furthermore, this data agrees with a recent study showing that newly polymerizing actin can mobilize active β1 integrin at the leading edge of motile cells (Galbraith et al., 2007).

β3 integrin promotes VASP phosphorylation

For cells to undergo persistent motility, adhesion dynamics must also be coordinated with assembly of new F-actincontaining protrusions, which are in turn under the control of several actin-nucleating and elongating molecules (Le Clainche and Carlier, 2008). One such family are the Ena/VASP proteins, which act to antagonize capping protein to induce actin filament elongation (Sechi and Wehland, 2004) and localize to focal adhesions. To identify the potential signaling proteins responsible

for regulating actin dynamics downstream of β3, we adopted a candidate approach to test for levels and localization of several adhesion and actin regulatory proteins in WT and $\beta 3-/-$ cells. One of the most striking differences was in the phosphorylation of VASP. Western blot analysis for VASP demonstrated an almost total loss of S153 phosphorylation in cells lacking \(\beta \) compared with that in WT cells or $\beta 3-/-$ cells rescued with human β3-GFP (Fig. 3 A; quantified in Fig. 3 B). VASP is known to be serine-phosphorylated by protein kinase A (PKA) during cell spreading (Howe et al., 2002). Phosphorylation of VASP at both S153 in mice (or S157 in humans) and S235 has also been shown to promote actin filament assembly in vitro (Barzik et al., 2005). More recent studies have also shown that VASP phosphorylated at S157 accumulates at the cell periphery in platelets and in spreading cells (Wentworth et al., 2006; Benz et al., 2009). However, the role of VASP phosphorylation in regulating focal adhesion protein behavior is unclear. Western blot analysis additionally showed that VASP S153 phosphorylation levels were reduced after PKA inhibition by H89, and an activator of PKA signaling (Forskolin) was able to in part rescue S153 phosphorylation of VASP in $\beta 3-/-$ cells (Fig. 3, A and B). Conversely, phosphorylation of VASP S235 was unchanged between cell types (Fig. S3 B). Total levels of PKA RII regulatory subunit and PKA-dependent phospho-substrates were unchanged between cells types (Fig. S3 A), which suggests that β3 regulates local rather than global PKA activation. Interestingly, \(\beta 1 \) integrin-null cells did not show changes in VASP phosphorylation. Moreover, phosphorylation of the related family member Mena was unchanged between WT and β1-/- or β 3-/- cells (as also detected by phospho-specific antibodies), which suggests that VASP may be specifically acting downstream of \(\beta \) integrin (Fig. 3 A and not depicted). Knockdown of endogenous β3 by siRNA in human dermal fibroblasts also resulted in decreased levels of phosphorylated VASP, which suggested that the differences observed in the $\beta 3$ -/- cells were not caused by compensatory mechanisms (Fig. S3 C).

Confocal analysis of the localization of endogenous VASP in WT and $\beta 3-/-$ cells showed that VASP was recruited to small, peripheral adhesions in the WT cells, whereas VASP was absent from these adhesions in cells lacking β3 (Fig. 3 C). Confocal analysis of endogenous phospho-VASP also demonstrated predominant localization to the periphery of WT and β3-GFP cells, but very low signal in $\beta 3-/-$ cells (Fig. S3 D). To analyze the dynamics of VASP, WT, and $\beta 3-/-$, cells were transfected with GFP-WT VASP, and the protein was subjected to FRAP analysis. Surprisingly, analysis of recovery in peripheral adhesions in each cell type revealed significantly slower recovery $(\tau_{1/2})$ of VASP in $\beta 3-/-$ cells (Fig. 3 D). To determine the contribution of S153 phosphorylation to the dynamics of VASP, FRAP analysis was also performed on both WT and $\beta 3-/$ cells expressing GFP-S153A VASP (to mimic a de-phospho form of VASP). A significant increase in the $\tau_{1/2}$ recovery time of S153A VASP was seen compared with WT VASP in WT cells (Fig. 3 D), which suggests that dephosphorylation of VASP at this site results in increased residence time of the protein within peripheral adhesions. To determine whether loss of B3 also affected dynamics of other focal adhesion proteins, we performed

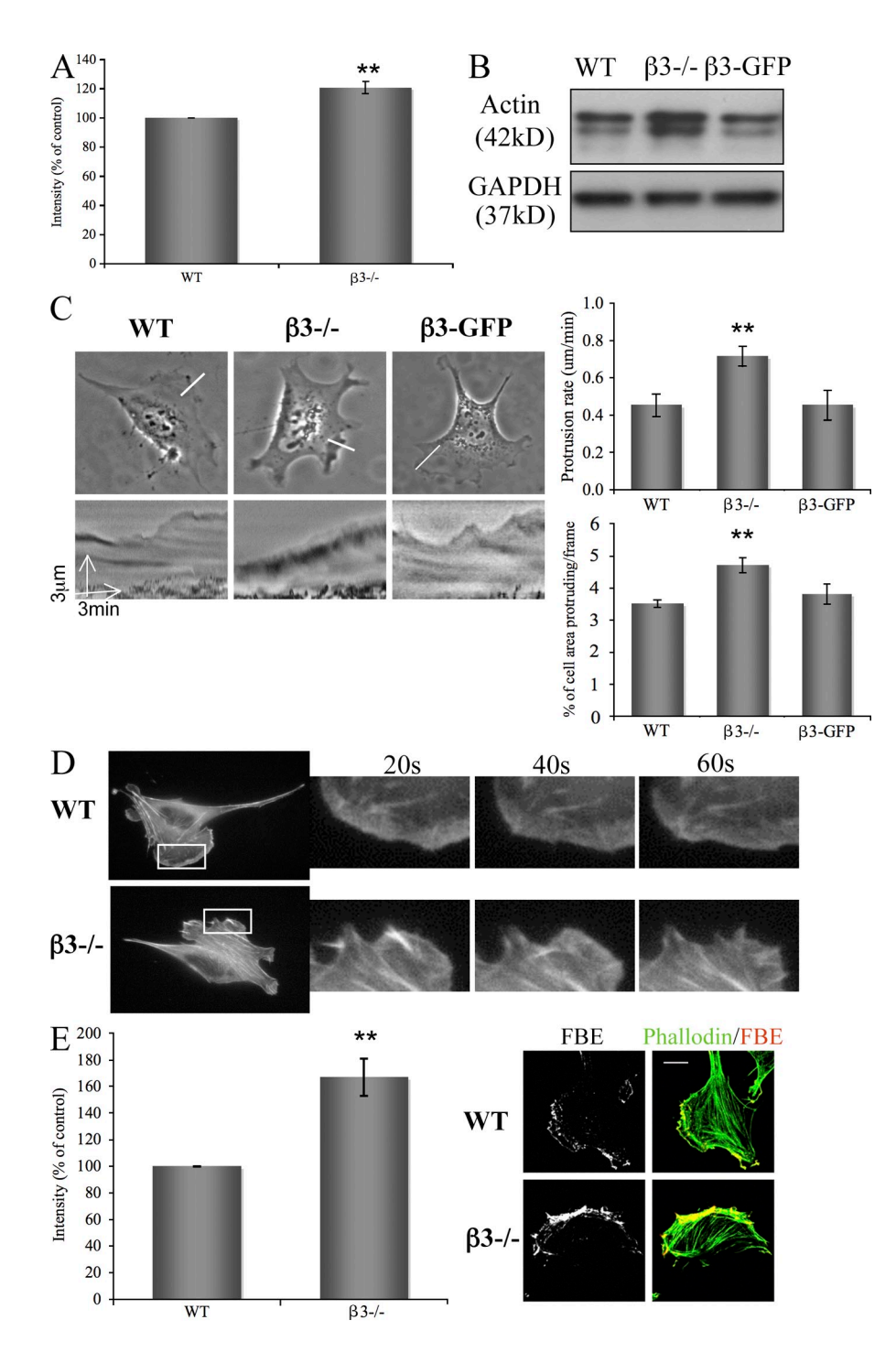


Figure 2. Loss of **B3** results in formation of unstable actin protrusions. (A) WT and β 3-/- cells analyzed for total F-actin content by FACS analysis of phalloidin staining intensity. Data are presented as the percentage intensity of WT control cells ± SEM pooled from three independent experiments (indicated by error bars). (B) WT, $\beta 3-/-$, or $\beta 3$ -GFP cell lysates from TX-100 insoluble fractions analyzed by Western blotting for β-actin or GAPDH as a loading control. Graphs are representative of four experiments. (C) Kymography analysis of protrusion rate and the percentage of cell area protruding/frame from time-lapse videos. Still images and example of kymographs obtained from the example white lines are shown on the left. Six lines were quantified from 12 cells over three independent experiments. Data are mean ± SEM (indicated by error bars). (D) WT and $\beta 3-/-$ cells transfected with GFP-actin and imaged by fluorescence timelapse microscopy. Stills are shown from an example of each cell type, enlarged images of protruding regions of membrane over time (boxes) are shown on the right. (E) Quantification and example images of free barbed end formation in WT and $\beta 3-/-$ cells. Live cells were pulsed with Alexa Fluor 568-G-actin (red) for 1 min, fixed, and stained with phalloidin-488 (green). The intensity of G-actin incorporation was quantified from at least 100 cells from three independent experiments. Data are shown as the mean percentage intensity ± SEM compared with WT control (indicated by error bars). *, P < 0.01. Bars, 10 µm.

FRAP analysis on both WT and $\beta 3$ –/- cells expressing GFP-talin or GFP-vinculin. Interestingly, data demonstrated a significant increase in the $\tau_{1/2}$ recovery time of talin in the $\beta 3$ –/- cells compared with WT (Fig. 3 E). Conversely, vinculin demonstrated similar recovery kinetics in both cell types (Fig. 3 E). This suggests that $\beta 3$ integrin is specifically involved in regulating VASP and talin dynamics at adhesions. To further examine the relationship between specific integrin populations and talin recovery, we performed FRAP analysis on talin-mCherry expressed in $\beta 1$ -GFP or $\beta 3$ -GFP (expressed in respective null integrin backgrounds)–positive adhesions. Data revealed that talin recovery was significantly slower at $\beta 1$ - versus $\beta 3$ -rich

adhesion sites (Fig. 3 F), which suggests that integrin-specific signals can act to differentially regulate talin dynamics.

β 3 integrin restricts VASP binding to RIAM

To better understand how phosphorylation of VASP at S153 may be affecting subcellular localization of VASP, we expressed GFP-tagged WT, S153D, or S153A VASP in WT cells and analyzed localization with respect to active $\beta1$ integrin in fixed cells. Confocal images demonstrate partial colocalization between both WT and S153D VASP and active integrin at focal adhesions but not at the leading edge of new protrusions

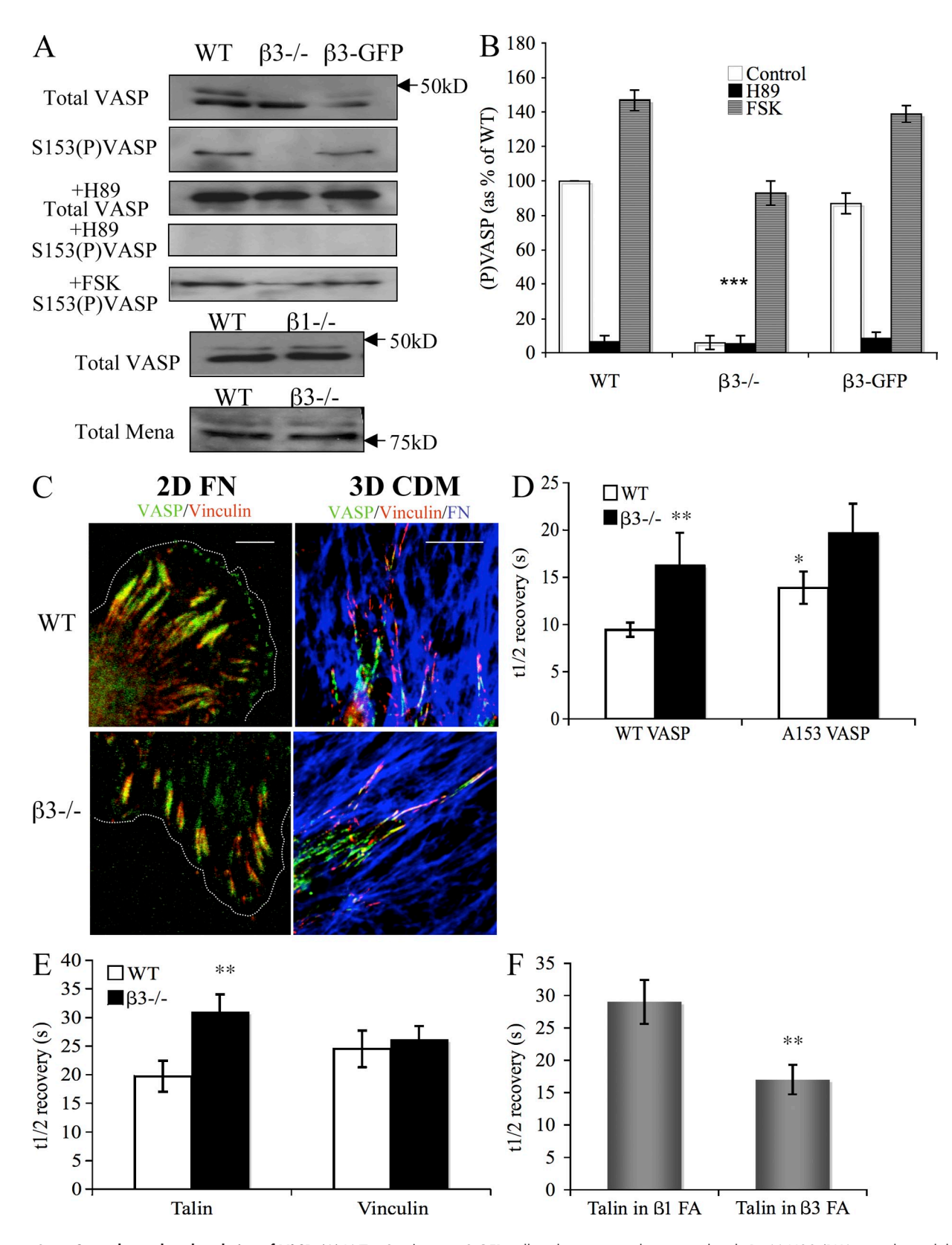


Figure 3. β 3 regulates phosphorylation of VASP. (A) WT, β 3-/-, or β 3-GFP cells either untreated or treated with 1 μ M H89 (PKA signaling inhibitor) or 1 μ M forskolin (PKA signaling activator) were analyzed by Western blotting for total VASP, phospho-S153 VASP, or total Mena. WT and β 1-/- cells were lysed and analyzed by Western blotting for total VASP. (B) Quantification of blots from WT, β 3-/-, or β 3-GFP cells shown in A. Data are mean \pm SEM from four independent experiments (indicated by error bars). ***, P < 0.001 compared with WT control levels. (C) Confocal images of WT and β 3-/- cells plated on 2D FN (left; the dotted lines indicate the edge of the cells) or CDM (right) and stained for VASP (FITC, green), vinculin (Alexa Fluor 568, red), and FN (CDM only, Alexa Fluor 633, blue). Merged, enlarged images are shown. Bars: (left) 5 μ m; (right) 10 μ m. (D) WT and β 3-/- cells transfected with WT-VASP-GFP or S153A-VASP-GFP and subjected to FRAP analysis. $\tau_{1/2}$ values (s) were obtained from normalized recovery data for each construct in each cell type. Data are shown as mean values \pm SEM (indicated by error bars) from at least 10 cells from four independent experiments.

(Fig. 4 A). S153A VASP, however, showed markedly higher colocalization, with the majority of active integrin seen within focal adhesions, and this was confirmed by quantification using Pearson's correlation coefficient analysis (Fig. 4 A). VASP is a known binding partner for several focal adhesion proteins, including vinculin, αII spectrin, zyxin, and the MRL family protein RIAM (Brindle et al., 1996; Lafuente et al., 2004; Benz et al., 2008). As our data demonstrates that loss of β3 promoted retention of VASP within β1-containing focal adhesions, we reasoned that this could be caused by increased binding of VASP to a focal adhesion protein. To test this hypothesis, we immunoprecipitated endogenous VASP from WT, β3-/-, or β3-GFP rescued cells and probed the bound fractions for associated focal adhesion proteins. Vinculin, αΠ spectrin, and zyxin coimmunoprecipitated with VASP at equal levels in all cell types (Fig. S4 A). Conversely, levels of RIAM were strikingly higher in complex with VASP in lysates from $\beta 3-/-$ cells as compared with WT or β3-GFP-rescued cells, whereas total RIAM levels were unchanged between cell lysates (Fig. 4 B). To test whether the increased binding between VASP and RIAM seen in $\beta 3$ —/— cells was caused by loss of phosphorylation on VASP S153, ectopically expressed GFP-tagged WT, S153A, or S153D VASP was immunoprecipitated from cells, and complexes were probed for the presence of endogenous RIAM. Data showed that RIAM was associated at higher levels with S153A versus WT VASP, which supports our hypothesis that phosphorylation of this residue can indeed regulate binding to RIAM (Fig. S3 E).

To analyze this enhanced interaction in vivo, we coexpressed GFP-VASP and RIAM-mCherry in WT and β3-/cells and analyzed direct interactions between these proteins by fluorescence resonance energy transfer (FRET) using fluorescence lifetime imaging microscopy (FLIM). This technique allows analysis of protein-protein interactions between a donor (GFP) and acceptor (mCherry) by measuring the fluorescence lifetime decay of the donor by time-correlated single photon counting. When donor and acceptor are in close proximity (<10 nm), energy transfer results in a shortening of the GFP fluorescence lifetime (Parsons et al., 2008; Worth and Parsons, 2008). Analysis of FRET lifetime images and cumulative FRET efficiency data (Fig. 4 C) confirmed that direct binding between VASP-RIAM was enhanced in β3-/- cells when compared with WT. Moreover, the interacting (FRET) population in β3-/- cells was predominantly at the cell periphery, compared with within discrete regions beneath the cell body in WT cells. Confocal analysis of endogenous active \(\beta 1 \) and RIAM localization in β3-GFP rescue cells also revealed colocalization between \(\beta \)1 and RIAM, whereas both proteins were absent from β3-containing peripheral adhesions (Fig. S4 B). Furthermore, analysis of FRET between RIAM-GFP and talin-mCherry in WT and $\beta 3$ —/— cells also demonstrated a significant increase in the

interaction between these proteins in cells lacking $\beta 3$ (Fig. 4 D). These data together suggest that loss of $\beta 3$ promotes enhanced association of a complex containing VASP, RIAM, and talin.

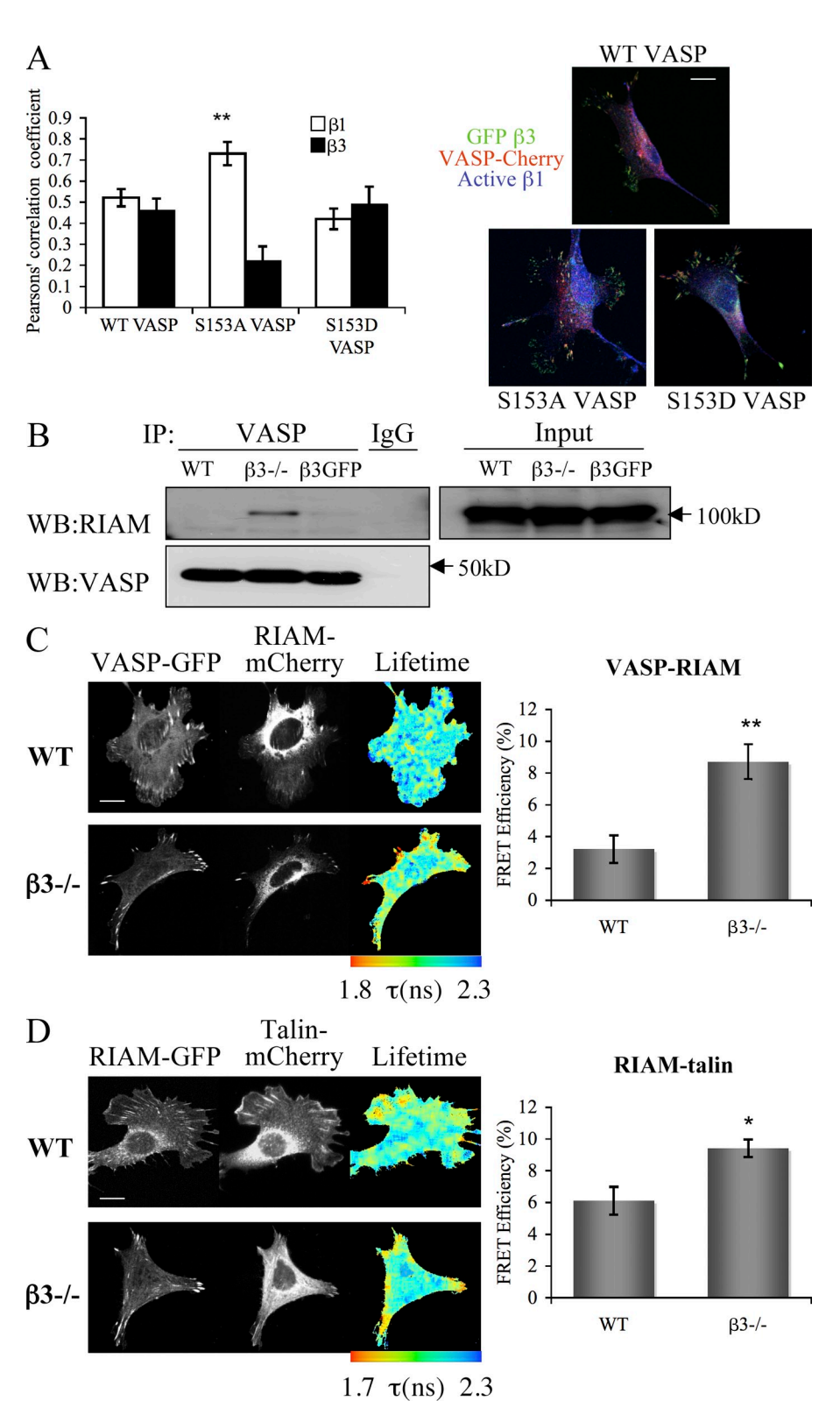
Phosphorylation of VASP regulates β1-talin binding

To further investigate whether VASP regulation of RIAM-talin binding had any downstream effect upon talin-integrin association, we used our previously established model to measure FRET between β 1-GFP (expressed in β 1-/- fibroblasts) and talin-mCherry (Parsons et al., 2008). As shown in lifetime images and FRET efficiency histograms (Fig. 5, A and C), coexpression of a myc-tagged form of S153A VASP in these cells led to a significant increase in the interaction between β1-GFP and talin compared with cells expressing endogenous or overexpressed WT VASP-myc. To reconfirm our findings that a β3 integrin-dependent VASP-RIAM signaling event acts to negatively regulate β1-talin binding, we knocked down endogenous β3, VASP, or RIAM in β1-GFP cells using siRNA/small hairpin RNA (Fig. S3 F) and measured binding between β1 and talin by FRET. Lifetime images and cumulative FRET efficiency analysis both demonstrate that a reduction in levels of β3 integrin promoted binding between \(\beta \) and talin; conversely, reduction of either RIAM or VASP led to a reduction in β1-talin binding (Fig. 5, B and C). Western blotting of β1-GFP cells expressing β3 siRNA also demonstrated a decrease in the higher molecular weight migrating species of VASP, confirming our findings that loss of β3 leads to loss of phosphorylated VASP at S153 (Fig. 3, A and B; and Fig. S3 F).

To determine whether the effects of VASP on integrin-talin binding translated into functional regulation of \$1 integrin dynamics, we performed FRAP analysis on \(\beta 1-GFP \) alone or in cells coexpressing WT, S153A, or S153D VASP-mCherry (Fig. 6, A and B). Interestingly, data demonstrated a significant decrease in the $\tau_{1/2}$ recovery time of $\beta 1$ in cells coexpressing S153A VASP compared with either control, WT, or S153D VASP-transfected cells (Fig. 6 B), which suggests that VASP phosphorylation status can alter both talin binding to $\beta 1$ and $\beta 1$ dynamics at adhesions. As loss of β3 integrin and/or loss of VASP S153 phosphorylation leads to increased activation of \$1, this would suggest that active β 1 demonstrates reduced $\tau_{1/2}$ recovery time in FRAP experiments. This is in contrast to the increased $\tau_{1/2}$ recovery time seen for talin in cells lacking \(\beta \) (Fig. 3 E). Interestingly, additional analysis of the immobile fraction of β 1-GFP in these experiments revealed an increase in the immobile fraction of \(\beta 1 \) in cells coexpressing S153A VASP compared with WT VASP (62.6% vs. 43.7%, respectively; P = 0.005). These novel observations also suggest a model whereby increased residence time of proteins within focal adhesions may be required to induce integrin activation, leading to increased dynamic recovery of the integrin itself within the same adhesion site.

^{**,} P < 0.01; *, P < 0.05 compared with WT VASP recovery in WT cells. (E) WT and $\beta3-/-$ cells transfected with talin-GFP or vinculin-GFP and subjected to FRAP analysis. $\tau_{1/2}$ values (s) were obtained from normalized recovery data for each construct in each cell type. Data are shown as mean values \pm SEM from at least 11 cells from three independent experiments. **, P < 0.01 compared with recovery in WT cells. (F) FRAP analysis of talin-mCherry recovery at GFP-positive adhesions in $\beta1$ -GFP or $\beta3$ -GFP cells. $\tau_{1/2}$ values (s) were obtained from normalized recovery data for each construct in each cell type. Data are shown as mean values \pm SEM from at least 14 cells from four independent experiments (indicated by error bars). **, P < 0.01 compared with recovery in $\beta1$ -GFP cells.

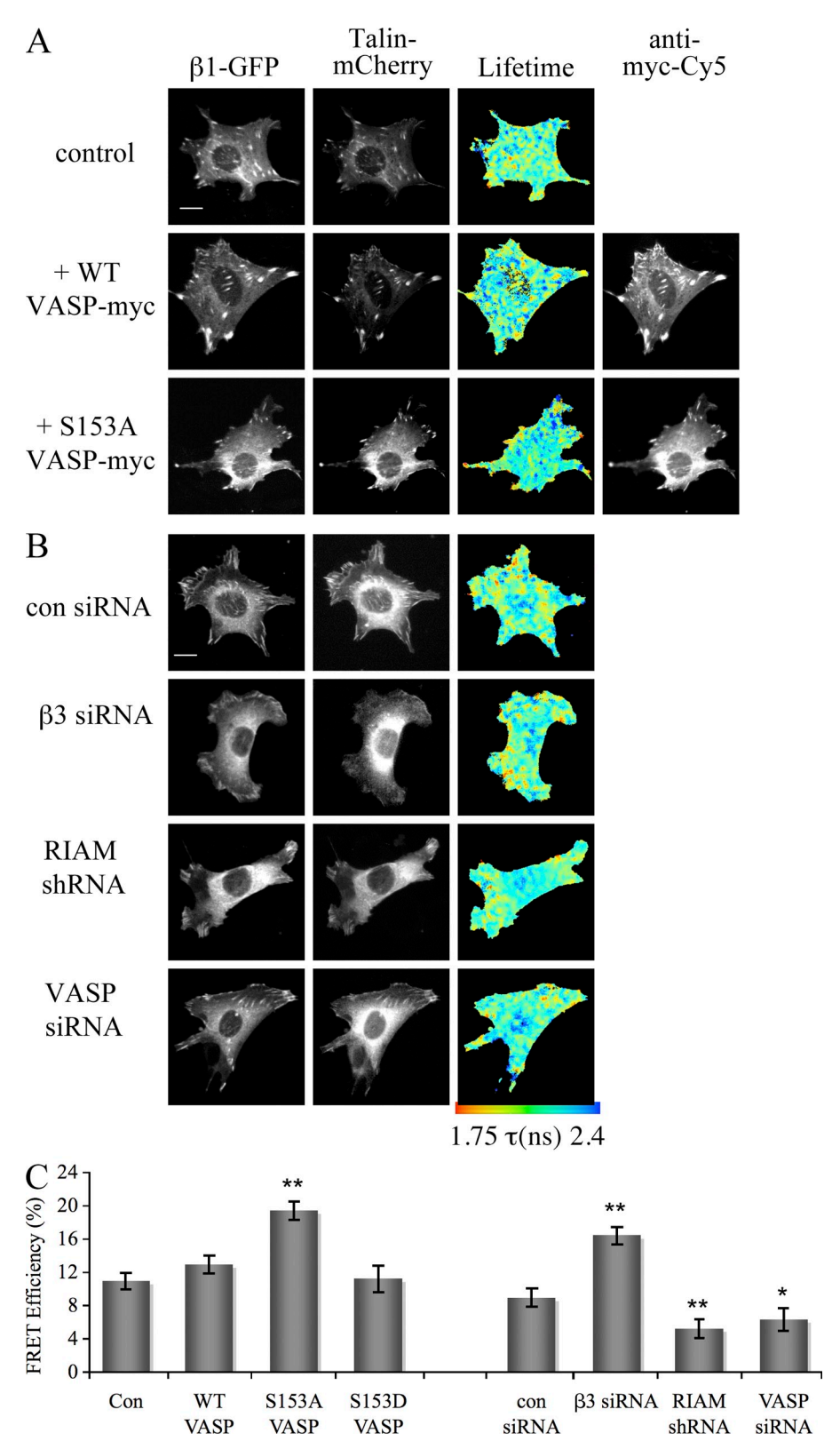
Figure 4. VASP-RIAM binding is enhanced in the absence of $\beta 3$. (A, right) Confocal images of β3-GFP cells transfected with WT, S153A, or S153D VASP-mCherry fixed and stained for active β1 (9EG7-Alexa Fluor 568, blue). Merged images are shown. Bars, 10 µm. (A, left) The histogram shows Pearson's correlation coefficient analysis of colocalization between VASP and 9EG7. Error bars indicate \pm SEM, n = 12 for each. **, P < 0.01. (B) WT, $\beta 3-/-$, or $\beta 3$ -GFP cells were lysed and subjected to immunoprecipitation with anti-VASP or control antibodies. Bound and input lysates were Western blotted for RIAM or VASP. Blots are representative of similar results from three independent experiments. (C, left) Example images of WT and $\beta 3-/-$ cells transfected with GFP-VASP alone (left, control) or in combination with mCherry-RIAM (right) subjected to FRET analysis by FLIM. Images show the GFP multiphoton intensity image and (where appropriate) corresponding wide-field image of the acceptor. Lifetime images mapping spatial FRET in cells are depicted using a pseudocolor scale (blue, normal lifetime; red, FRET). (C, right) Histogram of quantification of FRET efficiency from FLIM data. The graph represents mean FRET efficiency of >14 cells of each type over four independent experiments. Error bars indicate ± SEM. **, P < 0.01. (D) Example FRET images for WT and $\beta 3-/-$ cells transfected with GFP-RIAM and mCherry-talin. Quantification of FRET efficiency from FLIM data as in C. The graph represents mean FRET efficiency of >12 cells of each type over three independent experiments. Error bars indicate \pm SEM. *, P < 0.05. Bars, 10 µm.



VASP phosphorylation regulates adhesion dynamics and cell migration speed

Our data demonstrates that loss of $\beta 3$ results in increased adhesion turnover coupled with increased cell migration speed but with lower directional persistence. These phenotypes in $\beta 3-/-$ cells are coincident with decreased levels of S153-phosphorylated VASP. To determine whether $\beta 3$ -mediated signaling to VASP

plays a role in fibroblast adhesion dynamics, we measured rate constants of adhesion assembly and disassembly of GFP-talin expressed in WT, $\beta 3-/-$, or $\beta 3-/-$ cells expressing S153D VASP. Analysis revealed that the adhesion-enhanced assembly and disassembly seen in $\beta 3-/-$ cells was restored to WT levels in $\beta 3-/-$ cells expressing S153D VASP (Fig. 7 A). This suggests that forcing a balance of phosphorylated and



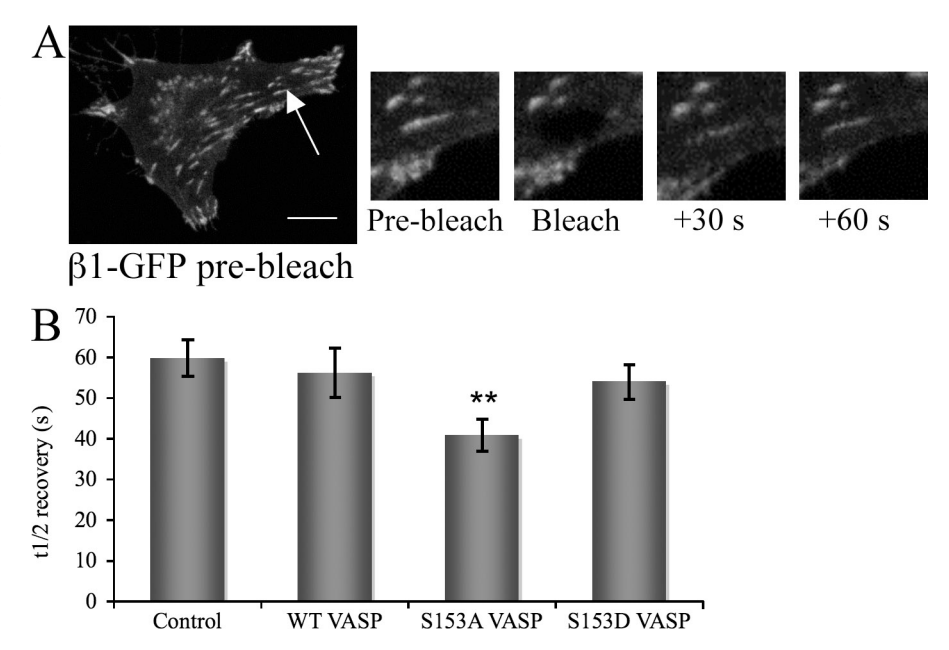
of β1-GFP-expressing fibroblasts cotransfected with mCherry-talin and either WT-VASPmyc or S153A VASP-myc. Cells were fixed and stained with an anti-myc-Cy5 antibody to detect VASP expression. Cells were then subjected to FRET analysis by FLIM. Images show the GFP multiphoton intensity image and (where appropriate) corresponding widefield image of the acceptor and myc-tagged VASP. Lifetime images mapping spatial FRET across the cells are depicted using a pseudocolor scale (blue, normal lifetime; red, FRET). Bars, 10 µm. (B) Example FLIM images of β1-GFP-expressing fibroblasts cotransfected with mCherry-talin and either control siRNA (con) or siRNA directed against B3 integrin, RIAM, or VASP. Cells were fixed and subjected to FRET analysis by FLIM. Images show the GFP multiphoton intensity image and corresponding wide-field image of the talin acceptor. Lifetime images mapping spatial FRET across the cells are depicted using a pseudocolor scale (blue, normal lifetime; red, FRET). (C) Quantification of FRET efficiency from FLIM data in A and B. The graphs represent mean FRET efficiency of >12 cells of each type over three independent experiments. Error bars indicate ± SEM. *, P < 0.05; **, P < 0.01.

Figure 5. **VASP regulates the interaction between β1 and talin.** (A) Example FLIM images

nonphosphorylated VASP is sufficient to restore normal adhesion dynamics in cells lacking $\beta 3$ integrin. To determine whether this rescue of adhesion kinetics was coupled with a rescue in migration, we performed phase-contrast time-lapse microscopy on WT or $\beta 3-/-$ cells expressing S153A or S153D VASP mCherry. Data shown in Fig. 7 B and Fig. S3 G demonstrate

that expression of S153D VASP did indeed partially decrease enhanced migration speeds seen in $\beta 3-/-$ cells. However, the decreased directional persistence in $\beta 3-/-$ cells was unchanged by expression of either VASP mutant. Interestingly, expression of S153A but not S153D resulted in increased speed and decreased migration persistence in WT cells. To determine whether

Figure 6. VASP phosphorylation regulates $\beta 1$ integrin dynamics. (A) Example images of FRAP analysis of $\beta 1$ -GFP before and after bleaching. The arrow denotes the region of interest subjected to photobleaching. Bar, 10 μ m. (B) Quantification of FRAP analysis of $\beta 1$ -GFP recovery in mock transfected (control) cells or those coexpressing WT, S153A, or S153D VASP-mCherry. $\tau_{1/2}$ values (s) were obtained from normalized recovery data for $\beta 1$ -GFP in each condition. Data are shown as mean values \pm SEM from 12 cells from three independent experiments (indicated by error bars). **, P < 0.01 compared with recovery in control cells.



this S153D VASP-induced rescue in migration speed was coupled with changes in activation of $\beta1$, we analyzed 9EG7 intensity in $\beta3$, VASP, or RIAM-depleted cells and $\beta3-/-$ cells expressing VASP mutants. Data demonstrated that $\beta3$ depletion in WT cells resulted in increased active $\beta1$, whereas expression of S153D VASP in $\beta3-/-$ cells lead to reduced active $\beta1$ compared with nonexpressing $\beta3-/-$ cells in the same samples (Fig. 7 C). This suggests that $\beta3$ -dependent regulation of adhesion dynamics, $\beta1$ activation, and migration speed are controlled at least in part through regulation of VASP phosphorylation. However, directional migration appears to be regulated by an additional $\beta3$ -dependent pathway.

Discussion

Our studies of \(\beta \)3-null fibroblasts have revealed that this integrin plays a role in locally suppressing activation of β1 integrin to promote efficient persistent cell protrusion and migration. We show that $\beta 3$ -/- cells have increased migration speed and rates of adhesion assembly/disassembly, coupled with increased cell surface levels of active \$1 integrin and decreased levels of phosphorylated VASP. Expression of a S153A mutant of VASP promotes formation of complexes between VASP, RIAM, and talin; increased residence times of talin within adhesions; and increased talin-dependent activation of \$1 integrin. \$153D VASP expression partially rescued levels of active \$1 and migration speed defects in β3-/- cells; however, no effect was seen on the loss of persistent migration. Based on this evidence, we propose a model (Fig. 7 D) whereby in normal migrating fibroblasts, β3 integrin localizes predominantly to peripheral adhesion sites, where it retains a pool of phospho-VASP through a PKA-dependent mechanism. Under these conditions, very little VASP is associated with RIAM, and RIAM instead associates with talin (and other binding partners) at β1-rich focal adhesions. However, loss of $\beta 3$ results in the loss of S153-phosphorylated VASP, thus promoting formation of a

VASP–RIAM–talin complex at peripheral β 1-containing adhesions, which results in enhanced activation of β 1, more rapid adhesion turnover, and increased speed of migration.

Transdominant inhibition between integrin β subunits has previously been suggested to occur as a result of competition for binding to talin (Calderwood et al., 2004). Our data would suggest that β 3 is able to act transdominantly upon β 1 integrin in fibroblasts, in part through a surprisingly direct pathway under the control of VASP that results in restricted spatial association between $\beta 1$ and talin. This data favors an active signaling-dependent rather than passive stoichiometry model that governs the local association between integrins and talin. Whether such a model also applies to the other recently characterized family of integrin-activation proteins, the kindlins, remains to be tested. Recent studies have suggested that β1 and β3 integrins require association with both talin and kindlins to assume a fully activated conformation (Ma et al., 2008; Harburger et al., 2009). Furthermore, filamin is an additional β integrin–binding protein that potentially competes with talin for binding to the integrin tails (Kiema et al., 2006) and can also bind to migfilin (Lad et al., 2008). The cooperation between these alternative integrin-binding partners in complex with one another remains poorly understood, and it is likely that the balance between such complexes plays a key role in regulating kinetics of integrin activation. It will be important to address in future studies whether β3 also plays a role in regulating spatial interactions between these proteins.

Our data demonstrates a role for VASP phosphorylation in regulating both binding of VASP to RIAM and control of integrin activation. Although VASP phosphorylation has been previously implicated in the regulation of actin polymerization in vitro, little is known about functional regulation of VASP binding partners after phosphorylation by PKA (Barzik et al., 2005). Interestingly, a recent study has shown that dephosphorylation of VASP at S153 may be required for the growth of adhesion strength during membrane retraction in microglia, which supports

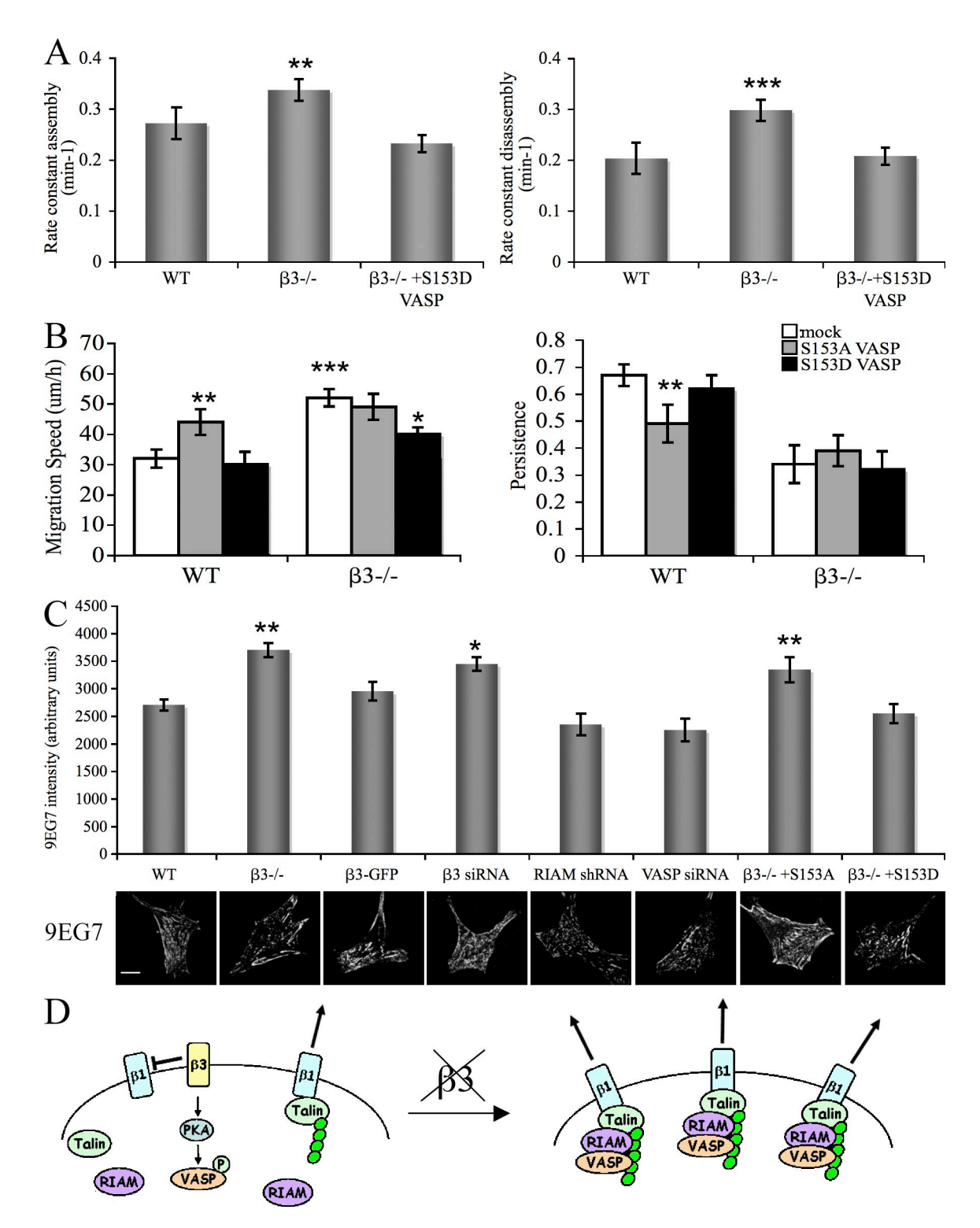


Figure 7. **Regulation of cell migration speed by VASP phosphorylation.** (A) Rate constants of focal adhesion dynamics in WT and $\beta 3-/-$ cells or $\beta 3-/-$ cells cotransfected with \$153D VASP-mCherry. Data are quantified from time-lapse videos of cells expressing GFP-talin. Data are expressed as min⁻¹ \pm SEM. Data were quantified from a minimum of 200 adhesions per condition over three experiments. (B) WT or $\beta 3-/-$ cells were mock transfected or transfected with \$153A or \$153D VASP-mCherry, plated onto FN-coated plates, and imaged using phase-contrast time-lapse microscopy over 16 h. Frames were taken every 10 min. Cells were tracked and migration speed and directional persistence were quantified as in Fig. 1. Data were quantified from >75 cells per condition over four independent experiments. Data are shown as mean \pm SEM (indicated by error bars). (C) Analysis of intensity levels of 9EG7 (active $\beta 1$) in cells expressing specified constructs. Example images of 9EG7 staining are shown underneath the graph for each sample type analyzed. Bars, 10 µm. 10 Error bars indicate \pm SEM. *, P < 0.05; **, P < 0.01; ***, P < 0.001. (D) Proposed model of $\beta 3$ regulation of $\beta 1$ activation through control of VASP, RIAM, and talin. In normal fibroblasts (left), the $\beta 3$ is located predominantly at the periphery of the cell, where it acts to maintain a local phosphorylated pool of VASP. In the absence of $\beta 3$ (right), VASP is predominantly dephosphorylated at \$153 (or \$157), leading to enhanced VASP binding to RIAM. This results in increased RIAM association with talin and enhanced talin binding to $\beta 1$ integrin, which leads to increased activation of $\beta 1$ at peripheral adhesion sites, increased cell protrusion, and faster, less persistent cell migration.

a role for VASP in regulation of integrin function (Lee and Chung, 2009). Previous biochemical studies have shown that RIAM is a binding partner for talin, and that formation of this complex can have a direct effect upon integrin activation (Lafuente et al., 2004; Han et al., 2006; Lee et al., 2009). More recently, an N-terminal helical motif within RIAM was identified as the putative binding sequence for talin, and coupling of this minimal sequence to the membrane-targeting domain of Rap1 was sufficient to induce activation of overexpressed $\alpha IIb\beta 3$ integrin (Lee et al., 2009). The same study reported that the VASP-binding site in RIAM (previously mapped to the C terminus of RIAM; Lafuente et al., 2004) was not required for RIAM to bind talin in vitro. However, as this study did not compare the ability of full-length versus VASP-binding mutants of RIAM to activate integrins, the observed positive contribution of VASP reported here remains a possible mechanism of regulation in other model systems. Furthermore, we cannot rule out the possibility that β3-dependent changes in Rap1 signaling may also be occurring in our model and possibly contributing to the enhanced β1-talin binding we observe in β3-null cells. Further detailed analysis of spatial activation of Rap1 will be required to determine the relative contribution of these pathways to β3-dependent regulation of RIAM and talin.

Our data also suggests that the integrin-dependent cycling of phospho-VASP may act to partition VASP into different compartments within the cell. Spatial control of VASP phosphorylation may in part be mediated through localized PKA activation. PKA can be activated in an integrin-dependent manner at the leading edge of migrating cells, and in the case of $\alpha 4\beta 1$ integrin, this effect is mediated directly through the ability of the integrin to act as an A-kinase anchoring protein (AKAP; Lim et al., 2007; Lim et al., 2008). In addition, β1 is known to activate and recruit phosphatases (Mutz et al., 2006; Gonzalez et al., 2008) and may therefore promote dephosphorylation of VASP. Our data suggests that this would lead to increased VASP residence time at adhesions, resulting in a RIAM-dependent positive feedback loop to increase β1 activation and adhesion turnover through cooperation with talin (Lafuente et al., 2004; Han et al., 2006; Lee et al., 2009). This model further strengthens our hypothesis that crosstalk between integrins is tightly regulated within discrete subcellular structures and that relatively minor changes to the dynamics of these key adhesion proteins can result in dramatic changes to cell protrusion and migration.

Data presented here also shows that $\beta 3$ —/— cells have increased formation of free barbed ends and enhanced assembly of F-actin—containing protrusions. The mechanism by which $\beta 3$ regulates actin assembly is currently unclear. Ena/VASP proteins have previously been shown to have potent effects on free barbed end formation (Furman et al., 2007; Philippar et al., 2008). The combined activity of VASP coupled to increased association of VASP with RIAM in the absence of $\beta 3$ provides one possible explanation for the increased barbed end formation in these cells. Rho GTPases are also primary targets for candidate downstream regulators, and in particular, regulation of the actin-severing protein cofilin by Rho represents one potential pathway by which integrins can regulate actin assembly. Conflicting studies in the literature suggest that engagement of

B3 integrin can both activate and inactivate cofilin under different conditions (Danen et al., 2005; Falet et al., 2005; White et al., 2007). Further experiments to study spatial regulation of cofilin and other actin regulatory proteins in integrin-null cells may provide more clues as to how these dynamic processes are regulated to separate adhesion assembly by integrin signaling during motility. Interestingly, our data would suggest that β3 can control focal adhesion assembly and migration speed in part through VASP, but that β3-dependent regulation of directed motility operates through an alternative and yet-undefined pathway. Uncoupling of these two distinct parameters has highlighted an additional layer of complexity in the cooperation between β1 and β3 integrins. Very few specific signaling events have been attributed to these seemingly functionally overlapping integrin β subunits within the same cellular context. Of note, one candidate that has received recent attention is the nonreceptor tyrosine kinase Src, which has previously been shown to bind directly to the cytoplasmic tail of β 3 (Arias-Salgado et al., 2003). This interaction is proposed to regulate \(\beta \)-dependent cell spreading and contractility as well as oncogenic transformation and anchorage-independent tumor cell growth (Flevaris et al., 2007; Huveneers et al., 2007; Desgrosellier et al., 2009). Src can phosphorylate several adhesion and cytoskeletal-associated substrates, and as such represents an attractive potential mediator downstream of β3 in the regulation of both F-actin assembly and migration persistence. Furthermore, proteomic-based screens to identify integrin-specific signaling complexes such as the one recently reported for $\alpha 4\beta 1$ and $\alpha 5\beta 1$ (Humphries et al., 2009) will provide additional novel targets for the dissection of functional differences between members of this receptor family within the same cell.

In summary, we have uncovered a novel VASP-dependent signaling mechanism downstream of $\beta 3$ integrin that contributes toward local inhibition of $\beta 1$ activation and regulates adhesion assembly and fibroblast migration speed. Our findings highlight the importance of dissecting such intricate, dynamic, and highly spatially regulated signaling networks to better understand the regulation of integrin-dependent adhesion and motility.

Materials and methods

Antibodies and reagents

Antibodies were obtained from the following suppliers: mouse anti-β-actin, anti-vinculin, anti-zyxin, and anti-talin (all from Sigma-Aldrich); mouse antitotal β1 and anti–rat active β1 (9EG7; both from Millipore); rabbit anti-β3 (AbD Serotec); mouse anti-paxillin (BD); FAK, FAK397(P), FAK 407(P), and FAK576(P) (all from Invitrogen); αll spectrin (a gift from P. Bennett, King's College London, London, England, UK); rabbit anti-FN (2413; Abcam); control IgG (Dako); glyceraldehyde 3-phosphate dehydrogenase (GAPDH; Sigma-Aldrich); rabbit anti-S157(P) VASP (3111; Cell Signaling Technol ogy); rabbit anti-VASP (2010) and mouse anti-RIAM (5541) as described in Lafuente et al. (2004); rabbit anti-PKA substrate antibody (Cell Signaling Technology); mouse anti-PKA RII antibody (Abcam); secondary HRP antibodies for Western blotting (all from Dako); and secondary fluorescently labeled antibodies (all from Invitrogen). G-actin-568 was obtained from Sigma-Aldrich, phalloidin-488 was obtained from Invitrogen, H89 and Forskolin were obtained from EMD; and human plasma FN was obtained from BD.

Constructs and siRNA

WT and mutant VASP constructs described previously (Barzik et al., 2005) were subcloned in GFP-C1 (Takara Bio Inc.) or mCherry-C1 (a gift from

R. Tsien, University of California, San Diego, La Jolla, CA) for imaging. GFP- and mCherry-talin were gifts from K. Yamada (National Institutes of Health, Bethesda, MD), and mRFP-vinculin was as described in Hashimoto et al. (2007). GFP-actin was as in Zicha et al. (2003). $\beta 3$ -GFP retrovirus was generated using human $\beta 3$ -N1-GFP (a gift from N. Kieffer, Centre National de la Recherche Scientifique/GDRE-ITI, University of Luxembourg, Luxembourg). The full $\beta 3$ -GFP sequence was amplified by PCR from the backbone using the following primers: (forward) 5'-CCCAAGCTTAT-GCGAGCGCGGCCG-3' and (reverse) 5'-CCCATCGATTTACTTGTA-CAGCTCG-3'. The PCR product was digested and ligated into the HindIII site (5') and Clal site (3') in pLCPX retroviral vector (Takara Bio Inc.). The construct was verified by sequencing before use. Control and On-target siRNA oligos against mouse VASP and mouse or human $\beta 3$ integrin were obtained from Thermo Fisher Scientific. The small hairpin RNA construct to RIAM was as described in Lafuente et al. (2004).

Cell culture and CDM preparation

Fibroblasts were isolated from WT and β3-null mice and immortalized in culture as described previously (Hodivala-Dilke et al., 1999). Cells were cultured in DME containing 10% FCS plus penicillin, streptomycin, glutamine, and 20 U/ml IFN- γ (all from Sigma-Aldrich) and maintained at 33°C and 5% CO₂. Cells isolated from at least five different animals for both WT and $\beta 3-/-$ were used throughout the studies. WT, $\beta 1$ -GFP, and β1-/- cells were derived and cultured in DME containing 10% FCS plus penicillin, streptomycin, glutamine, and 20 U/ml IFN-γ, as described previously (Parsons et al., 2008). Immortalized human dermal fibroblasts were cultured in α-MEM (Sigma-Aldrich) containing 10% FCS plus penicillin and streptomycin. CDMs were prepared as described previously (Cukierman et al., 2001; Caswell et al., 2007). In brief, gelatin-coated coverslips were cross-linked with glutaraldehyde, quenched, and equilibrated in DME containing 10% FCS. Primary human dermal fibroblasts (TCS Cellworks) were seeded at confluence and grown for 10-14 d in DME containing 10% FCS and 50 µg/ml ascorbic acid. Matrices were denuded of living cells by incubation with PBS containing 20 mM NH₄OH and 0.5% Triton X-100, and DNA residue was removed by incubation with DNasel. Matrices were blocked with 0.1% heat-denatured BSA before the seeding of cells.

Transfections and B3-GFP stable cell line generation

All transfections were performed using FuGene 6 reagent (Roche) or Dharmafect1 (for siRNA; Thermo Fisher Scientific) according to the manufacturer's instructions. Cells were plated at 50% confluency in 6-well plates and transfected using 0.5–2 $\mu g/well$ of DNA (depending on the construct used) or 5 nmol of siRNA suspended in Optimem (Invitragen). $\beta 3$ -GFP stable cells were generated by infecting $\beta 3$ -/ cells with $\beta 3$ -GFP retrovirus using AM12 packaging cells as described previously (Parsons et al., 2008). GFP-positive cells were selected by FACS and maintained under identical conditions to parent cells.

Immunoprecipitation and Western blotting

Cells were lysed in RIPA buffer (10 mM Tris, pH7.4, 150 mM NaCl, 1 mM EDTA, 1% Triton X-100, 1% sodium deoxycholate, 10 µM sodium fluoride, and 1 µM okadaic acid with protease inhibitor complex [EMD]). Cells were centrifuged at 13,000 rpm for 5 min, and lysate protein concentration was determined with the BCA assay (Thermo Fisher Scientific). For Western analysis, protein was loaded onto polyacrylamide gels and transferred to polyvinylidene fluoride membranes. Membranes were blocked in TBS-T and 5% nonfat milk, and incubated with the specified primary antibodies in TBS-T overnight at 4°C. The immunoblots were washed in TBS-T and incubated for 2 h with HRP-conjugated secondary antibodies. Membranes were then washed with TBS-T and visualized with ECL substrate reagent (Thermo Fisher Scientific). For immunoprecipitation, lysates were precleared with protein A/G beads (Santa Cruz Biotechnology, Inc.) and incubated with the indicated antibodies followed by incubation with protein A/G beads for 2 h at 4°C. Beads were washed three times in lysis buffer before being analyzed by Western blotting.

FACS

Cells were scraped into PBS on ice and centrifuged, and then the supernatant was removed. The cells were resuspended and incubated with phalloidin (1:100; Invitrogen) or 9EG7 (Millipore) on ice for 60 min. Cells were washed and resuspended where necessary in secondary antibody (Dako) and incubated on ice for 30 min. The supernatant was removed and the cells were resuspended in 250 µl of FACS Flow ready to be read by FACS Calibur (BD) using the CellQuest Pro version 4.0.2 software (BD).

Free barbed end assay and quantification of immunostaining

Analysis of actin free barbed-end formation was performed as described previously (Furman et al., 2007). In brief, cells were permeabilized with 0.125 mg/ml saponin in the presence of 0.5 mM Alexa Fluor 568–conjugated G-actin (Invitrogen). After a 2-min labeling period, samples were fixed in 0.5% glutaraldehyde, permeabilized with 0.5% Triton X-100, and blocked in the presence of Alexa Fluor 488–phalloidin (Invitrogen). Images were acquired using a microscope (A1R; Nikon) equipped with a CFI Plan-Fluor 40x oil objective lens. For quantification of 9EG7 intensity, coverslips were imaged using identical laser settings as for the free barbedend assay. In both experimental setups, look-up tables were used to ensure that pixel saturation was not reached, and the intensity per pixel was quantified using ImageJ software according to common background subtraction.

Live cell imaging and kymography

Phase-contrast imaging of cells was performed on a microscope (Axio100; Carl Zeiss, Inc.) equipped with a charge-coupled device camera (Sensicam; PCO), motorized stage (Ludl), excitation/emission filters (Chroma Technology Corp.) and filter wheels (Ludl). Images were acquired using a 40x oil objective (for single cell analysis) or 10x phase objective (for random motility). Kymography analysis of protrusion was performed using the ImageJ plugin (http://rsb.info.nih.gov/ij/). Six lines were quantified from 12 cells over three independent experiments.

Confocal microscopy, adhesion dynamics, and FRAP analysis

For all confocal experiments, cells were plated on glass coverslips coated with either 10 µg/ml FN or CDM as specified in the figure legends. Confocal microscopy and FRAP experiments were performed on a microscope (A1R; Nikon) equipped with a CFI Plan-Fluor 40x oil objective lens. Images were captured, analyzed, and exported using AR software (NIS Elements). Analysis of FRAP data was performed as in Humphries et al. (2007). In brief, raw intensity data were corrected for background fading during imaging and plotted as the percentage recovery over time, and $\tau_{1/2}$ values were calculated from the resultant curves. Data were pooled from at least 12 cells over five independent experiments. Focal adhesion dynamics were imaged and analyzed in transfected cells as described previously (Hashimoto et al., 2007). Rate constants of assembly and disassembly were determined from videos of cells expressing GFP-talin plated on either 2D FN or within CDM. Images were acquired on a confocal microscope (A1R). In the case of cells within CDM, rapid z stacks were acquired throughout the entire cell, and 3D projections were assembled before analysis. Rates of assembly and disassembly of adhesions were calculated by measuring the incorporation or loss of fluorescent signal of the protein over time. An increase in signal is a result of adhesion assembly and growth, whereas disassembly results in a loss of fluorescent signal. These intensity values were plotted over time on semilogarithmic graphs to provide a profile of intensity ratios over time. These ratios were calculated using the formula $I_n(I/I_0)$ for assembly and $I_n(I_0/I)$ for disassembly (where I_0 is the initial fluorescence intensity value and I is the intensity value for the relevant time point). Rates were then calculated from the gradient of the line of best fit.

FRET/FLIM

Fluorescence lifetime imaging was performed and data were analyzed as described previously (Parsons et al., 2008). We used FLIM to measure FRET between protein pairs, which allows the determination of spatial protein interactions. Time-domain FLIM was performed with a multiphoton microscope system as described previously (Parsons et al., 2008). Fluorescence lifetime imaging capability was provided by time-correlated single photon counting electronics (SPC 700; Becker & Hickl). A 40× objective was used throughout (CFI60 Plan-Fluor, NA 1.3; Nikon) and data were collected at 500 ± 20 nm through a bandpass filter (35-5040; Coherent, Inc.). Laser power was adjusted to give mean photon counting rates of the order 10^4 – 10^5 photons s - 1 (0.0001–0.001 photon counts per excitation event) to avoid pulse pileup. Acquisition times up to 300 s at low excitation power were used to achieve sufficient photon statistics for fitting, while avoiding either pulse pileup or significant photobleaching. Excitation was at 890 nm. Wide-field acceptor (mRFP) or Cy5 images were acquired using a charge-coupled device camera (Hamamatsu Photonics) at <100 ms exposure times.

Data were analyzed as described previously (Parsons et al., 2008) using TRI2 software (developed by P. Barber, University of Oxford, Oxford, England, UK). Histogram data presented here are plotted as mean FRET efficiency from >10 cells per sample. Mean FRET efficiency is shown ± SEM. Analysis of variance (ANOVA) was used to test statistical significance between different populations of data. Lifetime images of example

cells are presented using a pseudocolor scale whereby blue depicts normal GFP lifetime (no FRET) and red depicts lower GFP lifetime (areas of FRET).

Online supplemental material

Fig. S1 shows levels of focal adhesion proteins in WT and $\beta 3-/$ cells. Fig. S2 shows the percentage of dynamic adhesions in WT and β3-/- cells. Fig. S3 shows regulation of VASP phosphorylation in WT and $\beta 3-/-$ or $\beta 3$ -depleted cells. Fig. S4 shows regulation of ASP binding partners by $\beta 3$ integrin. Video 1 shows random migration of WT cells on 2D FN. Video 2 shows random migration of $\beta 3-/-$ cells on 2D FN. Video 3 shows migration of WT cells on CDM. Video 4 shows migration of $\beta 3-/-$ on CDM. Video 5 shows GFP-actin dynamics in WT cells on 2D FN. Video 6 shows GFP-actin dynamics in $\beta 3^{-}/-$ cells on 2D FN. Online supplemental material is available at http://www.jcb .org/cgi/content/full/jcb.200912014/DC1.

We would like to thank Nelly Kieffer and Ken Yamada for the kind gifts of reagents and Marjolein Snippe for technical assistance.

This work was supported by funding from the Royal Society (University Research Fellowship to M. Parsons), the Biotechnology and Biological Sciences Research Council (BBSRC; to M. Parsons and D.C. Worth) and National Institutes of Health grant GM50081 (to F.B. Gertler).

Submitted: 2 December 2009 Accepted: 21 March 2010

References

- Arias-Salgado, E.G., S. Lizano, S. Sarkar, J.S. Brugge, M.H. Ginsberg, and S.J. Shattil. 2003. Src kinase activation by direct interaction with the integrin beta cytoplasmic domain. Proc. Natl. Acad. Sci. USA. 100:13298-13302. doi:10.1073/pnas.2336149100
- Arnaout, M.A., S.L. Goodman, and J.P. Xiong. 2007. Structure and mechanics of integrin-based cell adhesion. Curr. Opin. Cell Biol. 19:495-507. doi:10.1016/j.ceb.2007.08.002
- Ballestrem, C., B. Hinz, B.A. Imhof, and B. Wehrle-Haller. 2001. Marching at the front and dragging behind: differential alphaVbeta3-integrin turnover regulates focal adhesion behavior. J. Cell Biol. 155:1319-1332. doi:10.1083/jcb.200107107
- Barzik, M., T.I. Kotova, H.N. Higgs, L. Hazelwood, D. Hanein, F.B. Gertler, and D.A. Schafer. 2005. Ena/VASP proteins enhance actin polymerization in the presence of barbed end capping proteins. J. Biol. Chem. 280:28653-28662. doi:10.1074/jbc.M503957200
- Benz, P.M., C. Blume, J. Moebius, C. Oschatz, K. Schuh, A. Sickmann, U. Walter, S.M. Feller, and T. Renné. 2008. Cytoskeleton assembly at endothelial cell-cell contacts is regulated by α II-spectrin-VASP complexes. J. Cell Biol. 180:205-219. doi:10.1083/jcb.200709181
- Benz, P.M., C. Blume, S. Seifert, S. Wilhelm, J. Waschke, K. Schuh, F. Gertler, T. Münzel, and T. Renné. 2009. Differential VASP phosphorylation controls remodeling of the actin cytoskeleton. J. Cell Sci. 122:3954-3965. doi:10.1242/jcs.044537
- Brindle, N.P., M.R. Holt, J.E. Davies, C.J. Price, and D.R. Critchley. 1996. The focal-adhesion vasodilator-stimulated phosphoprotein (VASP) binds to the proline-rich domain in vinculin. Biochem. J. 318:753-757.
- Broussard, J.A., D.J. Webb, and I. Kaverina. 2008. Asymmetric focal adhesion disassembly in motile cells. Curr. Opin. Cell Biol. 20:85-90. doi:10.1016/ j.ceb.2007.10.009
- Calderwood, D.A., V. Tai, G. Di Paolo, P. De Camilli, and M.H. Ginsberg. 2004. Competition for talin results in trans-dominant inhibition of integrin activation. J. Biol. Chem. 279:28889–28895. doi:10.1074/jbc.M402161200
- Caswell, P., and J. Norman. 2008. Endocytic transport of integrins during cell migration and invasion. Trends Cell Biol. 18:257-263. doi:10.1016/ j.tcb.2008.03.004
- Caswell, P.T., H.J. Spence, M. Parsons, D.P. White, K. Clark, K.W. Cheng G.B. Mills, M.J. Humphries, A.J. Messent, K.I. Anderson, et al. 2007. Rab25 associates with alpha5beta1 integrin to promote invasive migration in 3D microenvironments. Dev. Cell. 13:496-510. doi:10.1016/ i.devcel.2007.08.012
- Cukierman, E., R. Pankov, D.R. Stevens, and K.M. Yamada. 2001. Taking cell-matrix adhesions to the third dimension. Science. 294:1708-1712. doi:10.1126/science.1064829
- Danen, E.H., J. van Rheenen, W. Franken, S. Huveneers, P. Sonneveld, K. Jalink, and A. Sonnenberg. 2005. Integrins control motile strategy through a Rhocofilin pathway. J. Cell Biol. 169:515-526. doi:10.1083/jcb.200412081
- Desgrosellier, J.S., L.A. Barnes, D.J. Shields, M. Huang, S.K. Lau, N. Prévost, D. Tarin, S.J. Shattil, and D.A. Cheresh. 2009. An integrin

- alpha(v)beta(3)-c-Src oncogenic unit promotes anchorage-independence and tumor progression. Nat. Med. 15:1163-1169. doi:10.1038/nm.2009
- Falet, H., G. Chang, B. Brohard-Bohn, F. Rendu, and J.H. Hartwig. 2005. Integrin alpha(IIb)beta3 signals lead cofilin to accelerate platelet actin dynamics. Am. J. Physiol. Cell Physiol. 289:C819-C825. doi:10.1152/ ajpcell.00587.2004
- Flevaris, P., A. Stojanovic, H. Gong, A. Chishti, E. Welch, and X. Du. 2007. A molecular switch that controls cell spreading and retraction. J. Cell Biol. 179:553-565. doi:10.1083/jcb.200703185
- Furman, C., A.L. Sieminski, A.V. Kwiatkowski, D.A. Rubinson, E. Vasile, R.T. Bronson, R. Fässler, and F.B. Gertler. 2007. Ena/VASP is required for endothelial barrier function in vivo. J. Cell Biol. 179:761-775. doi:10.1083/jcb.200705002
- Galbraith, C.G., K.M. Yamada, and J.A. Galbraith. 2007. Polymerizing actin fibers position integrins primed to probe for adhesion sites. Science. 315:992-995. doi:10.1126/science.1137904
- Gonzalez, A.M., J. Claiborne, and J.C. Jones. 2008. Integrin cross-talk in endothelial cells is regulated by protein kinase A and protein phosphatase 1. J. Biol. Chem. 283:31849-31860. doi:10.1074/jbc.M801345200
- Han, J., C.J. Lim, N. Watanabe, A. Soriani, B. Ratnikov, D.A. Calderwood, W. Puzon-McLaughlin, E.M. Lafuente, V.A. Boussiotis, S.J. Shattil, and M.H. Ginsberg. 2006. Reconstructing and deconstructing agonistinduced activation of integrin alphaIIbbeta3. Curr. Biol. 16:1796-1806. doi:10.1016/j.cub.2006.08.035
- Harburger, D.S., M. Bouaouina, and D.A. Calderwood. 2009. Kindlin-1 and -2 directly bind the C-terminal region of beta integrin cytoplasmic tails and exert integrin-specific activation effects. J. Biol. Chem. 284:11485-11497. doi:10.1074/jbc.M809233200
- Hashimoto, Y., M. Parsons, and J.C. Adams. 2007. Dual actin-bundling and protein kinase C-binding activities of fascin regulate carcinoma cell migration downstream of Rac and contribute to metastasis. Mol. Biol. Cell. 18:4591–4602. doi:10.1091/mbc.E07-02-0157
- Hodivala-Dilke, K.M., K.P. McHugh, D.A. Tsakiris, H. Rayburn, D. Crowley, M. Ullman-Culleré, F.P. Ross, B.S. Coller, S. Teitelbaum, and R.O. Hynes. 1999. Beta3-integrin-deficient mice are a model for Glanzmann thrombasthenia showing placental defects and reduced survival. J. Clin. Invest. 103:229-238. doi:10.1172/JCI5487
- Howe, A.K., B.P. Hogan, and R.L. Juliano. 2002. Regulation of vasodilatorstimulated phosphoprotein phosphorylation and interaction with Abl by protein kinase A and cell adhesion. J. Biol. Chem. 277:38121-38126. doi:10.1074/jbc.M205379200
- Humphries, J.D., P. Wang, C. Streuli, B. Geiger, M.J. Humphries, and C. Ballestrem. 2007. Vinculin controls focal adhesion formation by direct interactions with talin and actin. J. Cell Biol. 179:1043-1057. doi:10.1083/ jcb.200703036
- Humphries, J.D., A. Byron, M.D. Bass, S.E. Craig, J.W. Pinney, D. Knight, and M.J. Humphries. 2009. Proteomic analysis of integrin-associated complexes identifies RCC2 as a dual regulator of Rac1 and Arf6. Sci. Signal. 2:ra51. doi:10.1126/scisignal.2000396
- Huveneers, S., I. van den Bout, P. Sonneveld, A. Sancho, A. Sonnenberg, and E.H. Danen. 2007. Integrin alpha v beta 3 controls activity and oncogenic potential of primed c-Src. Cancer Res. 67:2693-2700. doi:10.1158/0008-5472.CAN-06-3654
- Hynes, R.O. 2002. Integrins: bidirectional, allosteric signaling machines. Cell. 110:673-687. doi:10.1016/S0092-8674(02)00971-6
- Kiema, T., Y. Lad, P. Jiang, C.L. Oxley, M. Baldassarre, K.L. Wegener, I.D. Campbell, J. Ylänne, and D.A. Calderwood. 2006. The molecular basis of filamin binding to integrins and competition with talin. Mol. Cell. 21:337–347. doi:10.1016/j.molcel.2006.01.011
- Lad, Y., P. Jiang, S. Ruskamo, D.S. Harburger, J. Ylänne, I.D. Campbell, and D.A. Calderwood. 2008. Structural basis of the migfilin-filamin interaction and competition with integrin beta tails. J. Biol. Chem. 283:35154-35163. doi:10.1074/jbc.M802592200
- Lafuente, E.M., A.A. van Puijenbroek, M. Krause, C.V. Carman, G.J. Freeman, A. Berezovskaya, E. Constantine, T.A. Springer, F.B. Gertler, and V.A. Boussiotis. 2004. RIAM, an Ena/VASP and Profilin ligand, interacts with Rap1-GTP and mediates Rap1-induced adhesion. Dev. Cell. 7:585-595. doi:10.1016/j.devcel.2004.07.021
- Le Clainche, C., and M.F. Carlier. 2008. Regulation of actin assembly associated with protrusion and adhesion in cell migration. Physiol. Rev. 88:489–513. doi:10.1152/physrev.00021.2007
- Lee, S., and C.Y. Chung. 2009. Role of VASP phosphorylation for the regulation of microglia chemotaxis via the regulation of focal adhesion formation/maturation. Mol. Cell. Neurosci. 42:382-390. doi:10.1016/j.mcn.2009.08.010
- Lee, H.S., C.J. Lim, W. Puzon-McLaughlin, S.J. Shattil, and M.H. Ginsberg. 2009. RIAM activates integrins by linking talin to ras GTPase membranetargeting sequences. J. Biol. Chem. 284:5119-5127. doi:10.1074/jbc .M807117200

- Lim, C.J., J. Han, N. Yousefi, Y. Ma, P.S. Amieux, G.S. McKnight, S.S. Taylor, and M.H. Ginsberg. 2007. Alpha4 integrins are type I cAMP-dependent protein kinase-anchoring proteins. *Nat. Cell Biol.* 9:415–421. doi:10.1038/ ncb1561
- Lim, C.J., K.H. Kain, E. Tkachenko, L.E. Goldfinger, E. Gutierrez, M.D. Allen, A. Groisman, J. Zhang, and M.H. Ginsberg. 2008. Integrin-mediated protein kinase A activation at the leading edge of migrating cells. *Mol. Biol.* Cell. 19:4930–4941. doi:10.1091/mbc.E08-06-0564
- Ma, Y.Q., J. Qin, C. Wu, and E.F. Plow. 2008. Kindlin-2 (Mig-2): a co-activator of β3 integrins. J. Cell Biol. 181:439–446. doi:10.1083/jcb.200710196
- Mutz, D., C. Weise, N. Mechai, W. Hofmann, R. Horstkorte, G. Brüning, and K. Danker. 2006. Integrin alpha3beta1 interacts with I1PP2A/lanp and phosphatase PP1. J. Neurosci. Res. 84:1759–1770. doi:10.1002/jnr.21078
- Parsons, M., A.J. Messent, J.D. Humphries, N.O. Deakin, and M.J. Humphries. 2008. Quantification of integrin receptor agonism by fluorescence lifetime imaging. J. Cell Sci. 121:265–271. doi:10.1242/jcs.018440
- Philippar, U., E.T. Roussos, M. Oser, H. Yamaguchi, H.D. Kim, S. Giampieri, Y. Wang, S. Goswami, J.B. Wyckoff, D.A. Lauffenburger, et al. 2008. A Mena invasion isoform potentiates EGF-induced carcinoma cell invasion and metastasis. *Dev. Cell.* 15:813–828. doi:10.1016/j.devcel.2008.09.003
- Ramsay, A.G., J.F. Marshall, and I.R. Hart. 2007. Integrin trafficking and its role in cancer metastasis. *Cancer Metastasis Rev.* 26:567–578. doi:10.1007/ s10555-007-9078-7
- Reynolds, L.E., F.J. Conti, M. Lucas, R. Grose, S. Robinson, M. Stone, G. Saunders, C. Dickson, R.O. Hynes, A. Lacy-Hulbert, and K. Hodivala-Dilke. 2005. Accelerated re-epithelialization in beta3-integrin-deficient-mice is associated with enhanced TGF-beta1 signaling. *Nat. Med.* 11:167–174. doi:10.1038/nm1165
- Ridley, A.J., M.A. Schwartz, K. Burridge, R.A. Firtel, M.H. Ginsberg, G. Borisy, J.T. Parsons, and A.R. Horwitz. 2003. Cell migration: integrating signals from front to back. *Science*. 302:1704–1709. doi:10.1126/science.1092053
- Sechi, A.S., and J. Wehland. 2004. ENA/VASP proteins: multifunctional regulators of actin cytoskeleton dynamics. Front. Biosci. 9:1294–1310. doi:10.2741/1324
- Tadokoro, S., S.J. Shattil, K. Eto, V. Tai, R.C. Liddington, J.M. de Pereda, M.H. Ginsberg, and D.A. Calderwood. 2003. Talin binding to integrin beta tails: a final common step in integrin activation. *Science*. 302:103–106. doi:10.1126/science.1086652
- Vicente-Manzanares, M., C.K. Choi, and A.R. Horwitz. 2009. Integrins in cell migration—the actin connection. J. Cell Sci. 122:199–206. doi:10.1242/ jcs.018564
- Wentworth, J.K., G. Pula, and A.W. Poole. 2006. Vasodilator-stimulated phosphoprotein (VASP) is phosphorylated on Ser157 by protein kinase C-dependent and -independent mechanisms in thrombin-stimulated human platelets. *Biochem. J.* 393:555–564. doi:10.1042/BJ20050796
- White, D.P., P.T. Caswell, and J.C. Norman. 2007. α v $\beta 3$ and $\alpha 5\beta 1$ integrin recycling pathways dictate downstream Rho kinase signaling to regulate persistent cell migration. *J. Cell Biol.* 177:515–525. doi:10.1083/jcb.200609004
- Worth, D.C., and M. Parsons. 2008. Adhesion dynamics: mechanisms and measurements. *Int. J. Biochem. Cell Biol.* 40:2397–2409. doi:10.1016/ j.biocel.2008.04.008
- Zaidel-Bar, R., C. Ballestrem, Z. Kam, and B. Geiger. 2003. Early molecular events in the assembly of matrix adhesions at the leading edge of migrating cells. J. Cell Sci. 116:4605–4613. doi:10.1242/jcs.00792
- Zamir, E., M. Katz, Y. Posen, N. Erez, K.M. Yamada, B.Z. Katz, S. Lin, D.C. Lin, A. Bershadsky, Z. Kam, and B. Geiger. 2000. Dynamics and segregation of cell-matrix adhesions in cultured fibroblasts. *Nat. Cell Biol.* 2:191–196. doi:10.1038/35008607
- Zicha, D., I.M. Dobbie, M.R. Holt, J. Monypenny, D.Y. Soong, C. Gray, and G.A. Dunn. 2003. Rapid actin transport during cell protrusion. *Science*. 300:142–145. doi:10.1126/science.1082026